The Effect of ENSO Events on the Tropical Pacific Mean Climate: Insights from an Analytical Model

Jin Liang[1,2], Xiu-Qun Yang [1], and De-Zheng Sun [2*]

[1] *School of Atmospheric Sciences, Nanjing University, Nanjing 210093, China*

[2] *Cooperative Institute for Research in Environmental Sciences, University of Colorado and NOAA/Earth System Research Laboratory/Physical Science Division, Boulder, Colorado*

Corresponding author: Dr. De-Zheng Sun, Cooperative Institute for Research in Environmental Sciences, University of Colorado and NOAA/Earth System Research Laboratory/Physical Science Division, Boulder, Colorado.
Email: dezheng.sun@noaa.gov

ABSTRACT

To better understand the causes of climate change in the tropical Pacific on the decadal and longer time scales, we delineate the rectification effect of ENSO events into the mean state by contrasting the time-mean state of a low-order model for the Pacific with its equilibrium state. The model encapsulates the essential physics of the ENSO system, but remains simple enough to allow us to obtain its equilibrium state. The model has an oscillatory regime that resembles the observations. In this oscillatory regime, the time-mean SST in the eastern equatorial Pacific is found to be significantly different from the corresponding equilibrium SST, with the former being warmer than the latter. The difference is found to be proportional to the amplitude of ENSO. In addition, the zonal SST contrast of the time-mean state is found to be less sensitive to increases in external forcing than that of the equilibrium state, due to warming effect of ENSO events on the eastern Pacific. It is further shown this rectification effect of ENSO events owns to the nonlinear advection term in the heat budget equation. The study elucidates the role of ENSO events in shaping the tropical mean climate state and suggest that decadal warming in the recent decades in the eastern tropical Pacific may be more a consequence than a cause of the elevated ENSO activity during the same period. The results also provide a simple explanation for why it is difficult to detect an anthropogenically forced trend in the zonal SST contrast in the observations.

1. Introduction

The importance of the tropical Pacific sea surface temperature (SST) in predicting climate variability over North American and the world at larger has been vividly demonstrated in our rich experience with ENSO (Philander 1990). The apparent regime-like shift in the tropical Pacific SST from about 1976 has underscored another fact about tropical Pacific SST: it also varies on decadal time-scales (Wang and Ropelewski 1995; Zhang et al. 1997; Fedorov and Philander 2000). As the society increasingly needs a climate outlook beyond the time-scale of ENSO, understanding the mechanisms that give rise to the decadal variability in the background state of ENSO (or the time-mean state relative to the time-scale of ENSO) has become a forefront issue facing climate research community (Meehl et al. 2010).

This regime shift shown in Fig. 1a is accompanied with the change in the level of ENSO variability – the variance of the interannual variability of the tropical Pacific SST (Fig. 1b). The level of ENSO activity during the epoch with a warmer time-mean SST in the eastern tropical Pacific is anomalously higher than the previous epoch with a colder time-mean SST in the eastern tropical Pacific. Is the change in the level of ENSO activity caused by the change in the time-mean state, or the change in the time-mean state is a consequence of the change in the level of ENSO activity? A numbers of studies have examined the impact of a warming in the mean state of the tropical Pacific on the level of ENSO activity (Fedorov and Philander 2000, 2001; An and Jin 2001; and Wang and An 2001 among others). These studies employ the traditional linear instability analysis of the mean state and deduce the impact of changes in the mean state on the growth rate of the ENSO modes. These studies have nicely illuminated a consistency between the changes in the level of ENSO activity and the corresponding changes in the time-mean state, within the mathematical

framework of linear instability analysis. However, these studies do not address the cause of the warming in the time-mean state, in particular the question whether an increase in the level of ENSO activity can induce a warming in the time-mean state. We here employ a different methodology and explore the possibility that the decadal warming over the eastern Pacific is due to the rectification effect of elevated ENSO events into the mean state (i.e. the time-mean effect of ENSO events).

The possibility that ENSO may have an important time-mean effect on the tropical Pacific climatology has been highlighted by preliminary studies of the role of ENSO in the heat balance of the tropical Pacific. In a numerical experiment with a coupled model, Sun and Zhang (2006) found that the response in the upper ocean temperature to an increase in the tropical heating is very different between the case with ENSO and the case without ENSO. The presence of ENSO can increase considerably the response in the subsurface temperature, and shift the maximum surface level response from the western Pacific warm-pool to a broad region in the central and eastern Pacific. Sun and Zhang (2006) further noted that this time-mean effect of ENSO is linked to an asymmetric response to an increase in the tropical heating between the two phases of ENSO.

The surface manifestation of the asymmetry between El Niño and La Niña events – the strongest El Niño event, measured by the Niño3 SST anomaly, being stronger than the strongest La Niña event – has long been noted (Zebiak and Cane 1987; Burgers and Stephenson 1999). It has also been suggested by recent studies that decadal variability may result from a "residual" effect of ENSO on the background state due to the asymmetry between El Niño and La Niña events (Rodger et al. 2004; Sun and Yu 2009). Rodgers et al. (2004) found in a long simulation by a coupled GCM that changes in the mean state between decades with high ENSO activity and decades with

low ENSO activity resemble the residual of the two phases of ENSO in the model. They thereby suggest that the asymmetry could be a mechanism for decadal changes in the tropical Pacific SST. Noting a 15 year cycle in the level of ENSO activity in an extended SST data set consisting of historical and paleo-climate data, and a change in the asymmetry of ENSO with this decadal cycle, Sun and Yu (2009) has argued that the residual effect from the ENSO asymmetry may provide an explanation for the decadal cycle they have noted in the level of ENSO activity.

Specific mechanisms have also been proposed to explain the asymmetry between the two phases of ENSO. Jin et al. (2003) and An and Jin (2004) suggested that the asymmetry is due to the nonlinear term in the heat budget equation for the surface ocean. Schopf and Burgman (2006) showed that the skewness of the SST distribution could be due to a kinematic effect of oscillating a nonlinear temperature profile. While the relative contributions to the asymmetry between the two phases of ENSO from these two mechanisms need to be further studied, these studies suggest that the nonlinear aspects of ENSO are important, and a climate regime that has a higher level of ENSO activity may result in a different time-mean climate because the effects of stronger El Niño events may not be balanced by a corresponding change in the strength of the La Niña events.

Although the aforementioned studies are suggestive about a significant time-mean effect of ENSO on the climatology, this effect remains to be delineated clearly. We may divide the observations and model simulations of ENSO into epochs with different levels of ENSO activity and then try to discern the time-mean effect of ENSO by contrasting the mean states of these epochs as done in Rodgers et al. (2004), but this approach only confirms a correspondence between a change in the level of ENSO activity and a change in the mean state. The asymmetry between the two

117 phases of ENSO only suggests a non-zero residual effect of ENSO, to the extent that a
118 finite threshold value is used to define El Niño and La Niña events. But the
119 asymmetry alone is not a sufficient condition for a significant time-mean (or
120 rectification) effect of ENSO because such a residual effect will depend quantitatively
121 on how you define El Niño and La Niña events.

122 Ideally, we want to contrast the equilibrium state of the coupled tropical
123 ocean-atmosphere in which ENSO as an instability has not manifested with the actual
124 realized climatology in which ENSO has manifested. The difficulty for doing so is
125 that if the equilibrium state of the coupled tropical ocean-atmosphere is unstable, it is
126 by definition not observed. The same difficulty exists for complex GCMs whose state
127 evolutions have to be obtained by numerical integration of a set of equations which
128 also misses the unstable equilibrium state. In this paper, we present a low-order
129 analytical system for the coupled tropical ocean-atmosphere to explore the effects of
130 ENSO on the time-mean state. The model encapsulates the essential physics of ENSO
131 and has been shown to capture the major characteristics of ENSO (Sun 1997;
132 Timmerman and Jin 2002). The realized time-dependent state in the model can be
133 calculated numerically; the equilibrium state can be obtained analytically. Thereby,
134 we can delineate the role of ENSO events in the climatology (i.e., the time-mean state)
135 by comparing the two states. With this methodology, we will also be able to address
136 another question, which is whether ENSO plays a role in determining the sensitivity
137 of the climatology of the tropical Pacific to a change in external forcing. This
138 methodology we employ is analogous to that used by Manabe and his collaborators in
139 their attempt to establish the effect of moist convection on the mean climate – they
140 calculated the radiative equilibrium of their model atmosphere and compared with the
141 radiative convective equilibrium of their model atmosphere (Manabe and Moller 1961;

142 Manabe and Strickler 1964; Manabe and Wetherald 1967).

143 This paper is organized as follows. We first briefly describe the model in section 2.
144 We then present the main results concerning the differences between the time-mean
145 state and the equilibrium state in section 3. In section 4 we will discuss the asymmetry
146 of the oscillation in the model in connection with the differences between the
147 time-mean state and the equilibrium state. The nonlinearity responsible for the
148 rectification effect of ENSO events is isolated in section 5. Summary and discussion
149 are provided in section 6.

150

151 **2. The Model**

152 We use the model of Sun (1997, 2000). It is an extension of the model of Sun and
153 Liu (1996) by adding the thermocline dynamics in the manner given by Jin (1996).
154 The heat budget of the ocean surface layer can be written as

155 $$\frac{dT_1}{dt} = c(T_e - T_1) + sq(T_2 - T_1) \tag{1}$$

156 $$\frac{dT_2}{dt} = c(T_e - T_2) + q(T_{sub} - T_2) \tag{2}$$

157 $$s = \frac{U}{L_x} / \frac{W}{H_1} \tag{3}$$

158 where T_1 and T_2 represent the western and eastern equatorial Pacific surface
159 temperature, respectively; T_e is the radiative–convective equilibrium temperature;
160 $1/c$ is a typical thermal damping time scale; T_{sub} is the subsurface ocean temperature;
161 $q = W/H_1$, where W is the upwelling velocity in the equatorial eastern Pacific and H_1
162 is the depth of the mixed layer; zonal mass flux is assumed to be a fraction of the total
163 upwelling and this fraction can be measured by s. L_x in Eq. (3) represents the half
164 zonal width of the basin, and U represents the zonal velocity. The value of q is given

by

$$q = \frac{\alpha}{a}(T_1 - T_2) \tag{4}$$

where α measures the sensitivity of wind-stress to changes in the SST gradients; a defines the adjustment time scale of the ocean currents to surface winds. The subsurface temperature T_{sub} depends strongly on the eastern Pacific thermocline depth and can be parameterized as

$$T_{sub} = \Phi(-H_1 + h_2^{'}) \tag{5}$$

$$\Phi(z) = T_e - \frac{T_e - T_b}{2}(1 - \tanh(\frac{z + z_0}{H^*})) \tag{6}$$

$h_1^{'}$ and $h_2^{'}$ are the western and eastern equatorial thermocline anomalies; z_0 is the depth at which W takes its characteristic value. H^* measures the sharpness of the thermocline. T_b may be regarded as the temperature of the deep ocean. Following Jin (1996), $h_1^{'}$ and $h_2^{'}$ are governed by the following two equations:

$$h_2^{'} - h_1^{'} = -\frac{H_1}{H_2} H \frac{\alpha}{b^2}(T_1 - T_2) \tag{7}$$

$$\frac{1}{r}\frac{dh_1^{'}}{dt} = -h_1^{'} + \frac{H_1}{2H_2} H \frac{\alpha}{b^2}(T_1 - T_2) \tag{8}$$

A balance between zonal pressure gradients and zonal wind stress is shown in Eq. (7). H_2=H–H_1 with H being the zonal mean depth of the upper ocean at rest. b=c_k/L_x where c_k is the speed of the first baroclinic Kevin wave. A slow adjustment process of the thermocline depth to its equilibrium value determined by the surface wind-stress and mass conservation is adopted in Eq. (8). Parameter r in Eq. (8) measures the time scale for this slow adjustment process. As shown by Sun (1997) and Timmerman and Jin (2002), the model simulates the major characteristics of observed ENSO. Readers are referred to these two studies for temporal characteristics of the oscillation (i.e.,

time series of T_1, T_2, h_1' and h_2') simulated by the model. The focus of the present presentation is on the differences between the time-mean state and the equilibrium state of the model. We will discuss, however, the asymmetry of the oscillation in the model in relation to the differences between the time-mean state and the equilibrium state of the model.

3. The Differences between the Time-Mean State and the Equilibrium State

The time-mean state and the equilibrium state of the western equatorial Pacific SST (T_1) and the eastern equatorial Pacific SST (T_2) as a function of T_e are shown in Fig. 2a. The equilibrium state of the system has already been shown in Fig. 2 in Sun (1997); here we add the plot of time-mean state to contrast its difference from the equilibrium state. The parameters used here are the same as in Sun (1997). A standard Runge-Kutta method of fourth order is used to integrate the model equations and thereby obtain the time-mean state. The equilibrium state is obtained by setting the time derivatives on the left side of Eqs. (1), (2), (7) and (8) to zero, and then reducing Eqs. (1)–(8) to a single nonlinear algebraic equation.

As described by Sun (1997), Figure 2a shows that when the radiative forcing T_e achieves 25.5°C, a pitch-fork bifurcation (Strogatz 2001) of the system takes place and the coupled system starts to have SST gradients, winds, and currents. Further increasing T_e to 29.3°C, the system experiences a Hopf bifurcation (Strogatz 2001) and begins to enter an oscillatory state. The amplitude of the oscillation increases with further increase in T_e (Fig. 2b). The time-mean value and the equilibrium value of either T_1 or T_2 are the same before the occurrence of Hopf bifurcation, validating the accuracy of the numerical methods used to obtain the time-mean state. After the system enters the oscillatory regime, the two states are significantly different. The

time-mean value of T_2 (or T_1) in the presence of ENSO are observed to be larger than the corresponding equilibrium value under a given radiative forcing, and this discrepancy between the two values becomes even larger as we further increase the value of T_e to increase the amplitude of ENSO.

The difference in T_2 between the two states is much more profound than the difference in T_1. The two T_2 actually go to opposite directions as T_e increases in the presence of ENSO oscillation. The equilibrium T_2 decreases as T_e increases, a result that is reminiscent of that from Clement et al. (1996) [see also Cane et al. (1997)]. However, the time-mean value of T_2 increases with the increase of T_e. Note that in the present model, the background subsurface temperature is allowed to change in response to changes in T_e according to (5) and (6) while that in the Zebiak-Cane model (Zebiak and Cane 1987) – the model used by Clement et al. (1996) – is fixed. As discussed by Sun (2003) which employs an ocean model [the model of Gent and Cane (1989)] that has a heat budget for the subsurface ocean, the present approach implicitly takes into account the rectification effect of ENSO events into the reference subsurface temperature profile in a way that is consistent with the results from the more complicated ocean model used in Sun (2003).

For a given T_e, the time mean value of T_2 is much warmer than its equilibrium value. Correspondingly, the zonal SST contrast in the time-mean state is much reduced from that in the equilibrium state. Given the stability of the system is determined by the zonal SST contrast (Jin 1997; Sun 1997), the time-mean state is more stable than the equilibrium state. So the reason behind the warming effect of ENSO events on the eastern Pacific is that ENSO events tend to neutralize the equilibrium state. [Just in case it helps to bring this explanation to a general framework for what instability generally does to its mean state, we recall that tropical

deep convection collectively warms the upper troposphere and maintain a moist adiabatic lapse rate (Xu and Emanuel 1989). In other words, what ENSO events in the coupled ocean-atmosphere system do to the time-mean zonal SST contrast is analogous to what convective events in the tropical atmosphere do to the time-mean lapse rate].

Because the time-mean value of T_2 increases as T_e increases while the equilibrium T_2 actually decreases, the time-mean zonal SST contrast in the presence of ENSO increase at a much smaller rate than the equilibrium zonal SST contrast. The former is about 0.25^{o}C per 1^{o}C increase in T_e while the latter is 0.58^{o}C per 1^{o}C increase in T_e. This reduced sensitivity may explain the difficulty in detecting the anthropogenically forced increase in the zonal SST contrast in the observations (Vecchi et al. 2008): the data we have are yet good enough to detect this small change. We will return to this point in the summary section.

Differences between the time-mean subsurface ocean temperature T_{sub} and the equilibrium T_{sub} in the presence of ENSO oscillation are similar to those between the time-mean and the equilibrium T_2, but are more pronounced, consistent with the observations (Fig. 3a). The time-mean value of T_{sub} increases as T_e increases in the presence of ENSO, in contrast with its equilibrium solution which decreases. The relationship between T_{sub} and T_e shows even stronger nonlinearity than that between T_2 and T_e, indicating the importance of subsurface dynamics. As expected, the time-mean upwelling is less strong than that in the equilibrium state [recall Eq. (3)] (Fig. 3b). In the presence of ENSO, the depth of the thermocline in the east is deeper in the time-mean state than in the equilibrium state (Fig. 3c). The reverse is true for the thermocline in the west (Fig. 3d). As the amplitude of ENSO increases, the depth of the thermocline in the time-mean state in the east Pacific becomes increasingly

deeper than that in the equilibrium state, underscoring the impact of ENSO on the depth of the thermocline.

Using the same model, Timmermann and Jin (2002) showed that the temporal characteristics of the oscillation can be sensitive to the choice of s. For example, they found that a periodic solution described by Sun (1997) can become chaotic when the strength of zonal advection relative to the strength of the upwelling (the parameter s) is reduced while keeping the value of T_e fixed. We investigate whether the findings concerning the effect of ENSO on the tropical Pacific mean state depends on the details of ENSO characteristics by varying the value of s.

The case shown in Fig. 2 has the value of s set to 1/3. Figure 4 shows two more cases with s set respectively to 0 (a, b) and 0.096 (c, d). The two panels (a and b, or c and d) correspond to the two panels in Fig. 2. When we reduce the strength of zonal advection to be neglected (s=0), the two states of eastern equatorial Pacific SST T_2 again diverges after the Hopf bifurcation takes place and brings in the existence of ENSO. Note that Hopf bifurcation occurs at a much smaller value of T_e (T_e=26.8°C), indicating a stabilizing role from the existence of zonal advection. Unlike the case with s=1/3, the difference in T_2 between the two states in the case with s=0 doesn't increase monotonically as T_e increase. It comes to its maximum value at T_e=28°C, when the amplitude of ENSO reaches its maximum, and then decreases rapidly as the amplitude of ENSO decreases (Fig. 4b). The two states merges into a single one again at T_e=28.3°C when the oscillation disappears completely. This confirms that the differences between the two states are proportional to the amplitude of ENSO. Figure 4a shows clearly again that in the presence of ENSO, the time-mean T_2 is warmer than the equilibrium T_2. (i.e., the time mean state of the equatorial eastern Pacific in the presence of ENSO is warmer than the equilibrium state in which ENSO is

mathematically prevented from occurring). Figure 4c and 4d show the case with s=0.096, a value close to the one used by Timmermann and Jin (2002). Again, the results confirm the effect of ENSO on the mean state of the tropical Pacific: In the presence of ENSO, the two states are different with the time-mean T_2 warmer than the equilibrium T_2. Also, note that the regime of oscillation becomes wider as the value of s increases, presumably because zonal advection plays a stabilizing role as zonal advection is a cooling mechanism for the western Pacific. It has been shown by earlier studies that zonal advection is significant in observations and may play an important role in ENSO dynamics (Picaut et al. 1997; Fedorov and Philander 2001).

4. The Asymmetry of the Oscillation in the Model

The oscillation immediately after the Hopf bifurcation is regular. As the value of T_e further increases, the oscillation can become irregular. Fig. 5ab presents the time series of T_2 at T_e =28.5 ^{o}C and T_e =31 ^{o}C for the case with s=0.096. The equilibrium and time-mean values of T_2 are also added to the figure as horizontal lines to highlight the asymmetry of the oscillation and its possible connections with the differences between the equilibrium value and the time mean value. The figure shows that the system has a regular oscillation at T_e =28.5 ^{o}C (Fig. 5a) and an irregular oscillation at T_e =31 ^{o}C (Fig.5b).

In either the regime with regular oscillation or the regime with irregular oscillation, oscillations are asymmetric with respect to the time-mean value: the warm anomaly relative to the long-term time mean is not a mirror image of the cold anomaly relative the same long-term time mean. In the regime with regular oscillation, the main asymmetry is in the duration of the warm and cold events. The warm anomaly

312 (relative to the time-mean) lasts longer than the cold events. The asymmetry of the
313 oscillation is more profound measured by the departure from the equilibrium state. It
314 is interesting to see that the system lingers on the warmer side of the system longer
315 than its colder side. Note that the cold side has a stronger zonal SST contrast and
316 therefore a stronger current (recall Eq. (4)).
317
318 As the system enters the irregular regime, the main asymmetry is in the magnitude
319 of the warm and cold events (Fig. 5b). In the irregular regime, the system has weak
320 and strong warm events. The stronger warm events now have a larger amplitude than
321 the cold events. The cold events also vary in magnitude, but the variation is less than
322 in the magnitude of the warm events. The asymmetry in the irregular regime has a
323 close resemblance to the observed ENSO asymmetry (Burgers and DStephenson,
324 1999).
325 Relative to the equilibrium state, the asymmetry between the warm events and the
326 cold events in the irregular case is more profound. The equilibrium state almost sets
327 the limit how cold the system can get (Fig.5b). When the system does get to the colder
328 side, it quickly escapes to the warmer side. This asymmetry of the oscillation relative
329 to the equilibrium state is even more profound measured in the subsurface. Fig. 6a
330 shows the time series of h_1' that corresponds to Fig. 5b. The dashed line again denotes
331 the corresponding equilibrium value. Measured by h_1', the system rarely exceeds the
332 limit set by the equilibrium state. As found in Zhang et al. (2009), ENSO in the
333 observations also has a stronger asymmetry in its subsurface signature than the
334 surface signature. To highlight this impression, we further present in Fig. 6b the
335 trajectory of the system projected to the plan of T_2 and h_1' with the equilibrium state
336 and the time mean state also marked on the figure. It shows more vividly the

one-sided preference of the system relative to its equilibrium state. It suggests strongly that the rectification effect of ENSO into the time-mean state stems fundamentally from the asymmetry of the dynamics of the system relative to its equilibrium state.

The asymmetry of the dynamics of the system relative to its equilibrium point is consistent with the fact that the Hopf bifurcation (an instability) that brings the oscillation into being takes place *only* when the equilibrium state has a zonal SST contrast that is sufficient strong, and a depth of thermocline in the western Pacific that is sufficiently deep. In a sense, the zonal SST contrast may be regarded the thermal stress actually "felt" by the system, and the Hopf bifurcation (an instability) takes place when this "stress" is too strong to "bear". After breaking away from the equilibrium point through an instability, the system finds itself mostly on the more stable (or less stressful) side of its phase space—leading to a warmer eastern Pacific (and a reduced zonal SST contrast)---on average! This insight into the nature of ENSO—its asymmetry and its contribution to the time-mean state---will not be easily obtained if we do not subject the system to a gradually varying external thermal forcing as we have done here. In the next section, we explore which nonlinearity in the system that enables it to be capable of this seemingly "purposeful" behavior.

5. The Nonlinearity Responsible for Rectification

In addition to the nonlinear advection term in the system (the second term on the right hand of Eq. (2)), there is another source of nonlinearity—the reference temperature profile for the subsurface ocean (Eq. (6)) used to parameterize T_{sub} (Eq. (5)). With a linear profile is used, the rectification effect of ENSO events is found to

362 be equally profound (Fig. 7ab), indicating that it is the nonlinear advection term on
363 the right hand of Eq. (2) that provides the underlying mechanism for the rectification
364 effect.

365 The linear profile used to obtain Fig. 7 is the same used in the stability analysis of
366 Sun (1997, 2000),

367 $$\Phi(z) = T_{s0} + \gamma(z + H_1) \tag{9}$$

368 where $T_{s0} = \lambda T_e + (1-\lambda)T_b$ and $\gamma = (T_e - T_b)/2H_{ref}$. λ is a numerical constant. H_{ref} has
369 the dimension of depth. The corresponding Eq. (5) becomes

370 $$T_{sub} = T_{s0} + \gamma h_2^{'} \tag{10}$$

371 Fig. 7 shows the results corresponding to Fig. 2, but now with the linear profile Eq
372 (9) used to parameterize T_{sub} (Eq. (10)). As anticipated from the stability analysis of
373 Sun (2000), the system with a linear profile undergoes the same regime transitions as
374 the one with a nonlinear profile. As the value of T_e progressively increases, the system
375 first experience a pitch-fork bifurcation first to create the zonal SST contrast, then a
376 Hopf bifurcation when the zonal SST is sufficiently large. The system then starts to
377 oscillate and the time-mean solution and the equilibrium solution start to diverge. It is
378 evident that the warming effect of ENSO events on the eastern Pacific time-mean
379 state is equally profound in Fig. 7 as in Fig. 2. There are quantitative differences
380 between Fig. 2 and Fig. 7 even in the region immediately following the Hopf
381 bifurcation. Fig. 8 contrasts the nonlinear profile with the linear profile at T_e=29.5°C.
382 Note the two profiles have slightly different slope even in the region in the upper part
383 of the thermocline. The constants used in defining the linear profile are tuned to get a
384 Hopf bifurcation point that is close to that with the tangent profile, not to match the
385 lapse rate implied from the tangent profile at any particular depth.

386

With Eq. (9) replacing Eq. (6), it has been shown in Sun (2000) that the dynamic behavior of the system is controlled by the following 4 non-dimensional parameters: s, R, Λ, σ with the latter three parameter are given as (see Appendix II for details)

$$R = \frac{\alpha(T_e - T_{s0})}{ac} \tag{11}$$

$$\Lambda = p\kappa\gamma^* \tag{12}$$

$$\sigma = \frac{r}{c} \tag{13}$$

where $p = \frac{H_1}{2H_2}(1 + \frac{H_1}{H_2})$, $\kappa = \frac{ac}{b^2}$, $b = \frac{c_k}{L_x}$ with c_k being phase speed of the first baroclinic Kelvin wave and L_x is the half of the zonal width of the basin, and $\gamma^* = \gamma / \gamma_0$ with $\gamma_0 = (T_e - T_{s0}) / H_2$. (For convenience of reference, Appendix I lists the definition of all the symbols and parameters used in this article).

An exhaustive numerical exploration of the rectification effect in the entire parameter space is beyond the scope of the present study. We only present two situations here in which an analytical form for the rectification effect can be obtained to underscore the fundamental importance of the nonlinear advection term in Eq. (2) in giving rise to this effect. The details of the derivations are given in Appendix III.

With s=0, $\sigma = \frac{r}{c} >> 1$, it can be shown that

$$\overline{T_1} \approx T_{1eq} \tag{14}$$

$$\overline{T_2} \approx T_{2eq} + \frac{\overline{T_2'^2}}{\overline{T_1} - \overline{T_2}} \tag{15}$$

where over bar refers to time-mean, "*eq*" refers to equilibrium, and "$'$" detonates the anomaly above the time-mean (Details of derivation are given in Appendix III). Eq. (15) links the refection effect (the difference between the time-mean T_2 and the

equilibrium T_2 to the variance of the anomaly about the time-mean—the level of ENSO activity).

The simplest advective case (or convective case) (Fig. 9) – the situation considered in Sun (2000) and Schopf and Burgman (2006) as a thought experiment in which the eastern Pacific is periodically (or episodically with a 50% frequency) flooded by warm water due to an expanding warm-pool—appears to satisfy Eq. (15). In that situation, $\overline{T_1} \sim T_{1eq}$, $\overline{T_2} \sim \frac{1}{2}(T_{1eq} + T_{2eq})$, $\tilde{T}_2' \sim \overline{T}_1 - \overline{T}_2 \approx \frac{1}{2}(T_{1eq} - T_{2eq})$ with $\tilde{T}_2' = \sqrt{T_2'^2}$, a measure of the magnitude of T_2' (the anomaly about the time-mean).

For a more general value of σ, but with $\Lambda R >> 1$, we have

$$\overline{T_2} \approx T_{2eq} + \frac{\overline{T_2'^2}}{\overline{T}_1 - \overline{T}_2} \cos\beta \qquad (16)$$

where β is the phase difference between T_{sub} and T_2. The details of derivation are provided in the Appendix III. $\Lambda R >> 1$ corresponds to a situation with strong Bjerknes feedback, because

$$\Lambda R = \frac{H_1}{2H_2} H \frac{\alpha\gamma}{b^2} \qquad (17)$$

Recall that α and γ in Eq. (17) are respectively the coupling strength and the lapse rate of the thermocline (Appendix I).

Presenting Eq. (15) and Eq. (16) here is to further show that the rectification effect appears to be a robust property of the nonlineity in Eq. (2), and at least qualitatively does not appear to be sensitive to the choice of parameters.

6. Summary and Discussion

Motivated for a more complete understanding about the observed co-occurrences of an elevated (reduced) level of ENSO activity and a background warming (cooling) in the eastern tropical Pacific, we have employed a novel methodology to delineate the effect of ENSO events on the time-mean equatorial upper ocean. This new methodology is to contrast the time-mean state of a low-order nonlinear model with its equilibrium state. The realized time-dependent state in this model is calculated numerically, and the corresponding equilibrium state is obtained analytically, allowing us to compare the two states of coupled equatorial Pacific hand by hand, and thereby delineate the role of ENSO in shaping the tropical Pacific climatology.

The results from such an exercise show unambiguously that in the presence of ENSO, the differences between the equilibrium state and the realized time-mean state is significant. In particular, it is found that the time-mean equatorial eastern Pacific SST is significantly higher than that in the equilibrium state and that the time-mean zonal SST contrast is significantly weaker than that in the equilibrium state. The differences between the two states are further shown numerically to be proportional to the magnitude of ENSO oscillation.

The present results advance our understanding of the effect of ENSO events on the time-mean equatorial ocean beyond that from the empirical studies (Rodger et al. 2004; Sun and Yu 2009). This result, together with that from Sun and Zhang (2006) and Schopf and Burgman (2006) add weight to the argument that the recent decadal warming in the eastern tropical Pacific may be a consequence of the elevation of ENSO events during this period.

Although the present results strengthens the argument that the recent decadal warming in the eastern tropical Pacific may be a consequence of the elevation of ENSO events during this period, such a causality can not be firmly established unless

455 the causes of the elevation of ENSO activity are shown independent of the decadal
456 background warming in the tropical Pacific. As earlier studies have shown that a
457 decadal warming in the background state can cause an elevation of ENSO activity
458 (Fedorov and Philander 2000, 2001; An and Jin 2001; and Wang and An 2001), the
459 possibility is raised that a nonlinear interaction between ENSO events and the
460 time-mean state may act as a viable mechanism for decadal variability in the tropical
461 Pacific region. We note, however, the study by Wittenberg (2009) which shows that
462 the level of ENSO activity in a GFDL model can change substantially from one
463 decadal epoch to another without any notable change in the time mean state over the
464 epoch. We agree that there may be other causes for decadal variability in the level of
465 ENSO activity, such as random forcing from weather events. An interesting venue to
466 pursue is how the collective effect of weather events over the warm-pool influences
467 the decadal variability in the tropical maximum SST and thereby the decadal
468 variability in the value of T_e. We may not be conclude that the apparent lack of
469 rectification into the mean state in the GFDL model, contradict our conclusion here
470 also before we fully assess whether the ENSO events in the model is too linear
471 relative to what we see in observations (Sun et al. 2011). In fully assessing ENSO
472 asymmetry, it is important to examine its subsurface signatures (Zhang et al. 2009).
473
474 The analytical model also shows that at least in certain regimes, the amplitude of
475 ENSO events increase with enhanced radiative heating. Thus an interesting emerging
476 scenario is that ENSO events become stronger in response to an enhanced radiative
477 heating, which causes a warming in the tropical Pacific. Such a scenario is not
478 supported by coupled GCM simulations, however. A survey of coupled GCM
479 simulations has not revealed any systematic change in the level of ENSO activity in

response to global warming (Collins et al. 2010). This apparent contradiction may be again due to that the nonlinearity of ENSO is either nonexistent or severely underestimated by coupled GCMs (An et al. 2005; Sun 2010; Sun et al. 2011). Related to this consideration is the question whether the tropical Pacific region in the coupled GCMs is in the same dynamic regime as in the real world (Sun et al. 2006; Guilyardi et al. 2009; Guilyardi et al. 2011). Of course, it is also possible that the present model is too simple. A key issue ahead is to bridge the gap between simple models and GCMs in their predictions of the response of ENSO to global warming. Addressing this issue may necessarily entail a more critical assessment of the nonlinearity of ENSO events in the models including a quantification of the rectification effect of ENSO into the mean state in the various GCMs.

The results from the present analysis also suggest that the sensitivity of the tropical Pacific mean climate, the zonal SST contrast in particular, to an increase in the greenhouse effect, may be a function of the time-mean effect of ENSO events. The reduced rate of increase in the time-mean zonal SST contrast ($T_1 - T_2$) in the present model in response to an increase in the radiative-convective equilibrium SST (T_e), compared to that in the equilibrium state, suggests that the zonal SST contrast may be regulated by ENSO events. Whether this provides a viable explanation for the difficulty to detect a significant trend in the zonal SST contrast in the observations discussed by Vecchi et al. (2008) is a question worth exploring. In the same vein, recognizing this nonlinear effect of ENSO and the apparent inability to fully capture this effect by all the models may prove useful for fully understanding the differences among model predictions of the response of the zonal SST contrast to global warming. The results thus underscore the importance for climate models to correctly simulate ENSO, its nonlinear dynamics in particular, to be able to capture correctly the

505 response of the ENSO and the climatological state it determines.

506 We would like to note that the results reported in this article are from a highly
507 truncated version of the real coupled tropical Pacific ocean-atmosphere system. A
508 salient feature in the decadal warming of the east tropical Pacific (Fig. 1) is that the
509 maximum warming is not right on the equator. But the model in its current form does
510 not carry any information about the meridional structure of the rectification effect.
511 The results will have to be compared with those obtained by more sophisticated
512 models in order to fully ascertain the time mean effect of ENSO events. Regardless
513 the accuracy of the present results, the framework they constitute is likely to be useful
514 for diagnosing and understanding the results from more complicated climate models,
515 such as GCMs.

516 It has been suggested that ENSO variability may be simulated by a stable linear
517 system forced by weather noise (Penland and Sardeshmukh 1995, Penland 1996,
518 Moor and Kleeman 1999, Flugel et al. 2004, Kleeman 2008, among others). Indeed,
519 these models have performed remarkably well in simulating the SST anomalies
520 associated with ENSO events. Hence came the debate whether ENSO dynamics is
521 “linear” or “nonlinear”. It is often overlooked, however, that these studies take the
522 stability of the time-mean state as a given, and does not address the question why the
523 time-mean state appears to hover near the critical point. The present study may have
524 accidentally addressed this question and provided a potential underpinning for these
525 studies using anomaly models: ENSO events result from an instability of the
526 equilibrium state and through its time-mean effect, creates a stable or nearly stable
527 time-mean state. A subsequent study is planned to test this hypothesis. We also like to
528 include weather noise explicitly into the model to bridge the present work
529 quantitatively with those studies underscoring the role of noise in the irregularity of

530 ENSO. For now, the results from this simple nonlinear model shall help to underscore
531 the fact that the equilibrium state of the coupled tropical ocean-atmosphere may not
532 be the same as its time-mean state (i.e. the climatological state). With this difference
533 in mind, we have a reason to be hopeful that the gap between the two schools of
534 thoughts about the nature of ENSO dynamics may turn out to be not that big after all.
535

Appendix I: Definition of the symbols used in this study

T_e : the radiative–convective equilibrium temperature

T_b : deep ocean temperature

T_1 : equatorial western Pacific SST (120E-155W)

T_2 : equatorial eastern Pacific SST (155W-70W)

T_{sub} : subsurface temperature

H_1 : depth of the mixed layer

H : zonal mean depth of the upper ocean

$H_2 = H - H_1$

L_x : half width of the basin

u : zonal velocity

w : upwelling velocity

q : w / H_1

s : uH_1 / wL_x

$1/a$: adjustment time scale of the surface ocean currents to changes in the surface winds

$1/c$: time scale of removing a SST anomaly by surface fluxes

$1/r$: time scale of the slow adjustment in the ocean

α : sensitivity of the surface wind stress to changes in the SST gradients

$h_1^{'}$: deviation of the depth of the upper ocean in the western Pacific from its reference value H

$h_2^{'}$: deviation of the depth of the upper ocean in the eastern Pacific from its reference value H

c_k : phase speed of the first baroclinic Kelvin wave

b : c_k / L_x

p : $H_1 / 2H_2(1 + H_1 / H_2)$

κ : ac / b^2

σ : r / c

T_{s0} : characteristic value of the subsurface temperature

λ : parameter used to link T_{s0} with T_e and T_b through a linear extrapolation.

γ : lapse rate of the subsurface ocean

567 γ_0: $(T_e - T_{s0}) / H_2$, a reference lapse rate for the subsurface ocean.

568 γ^*: γ / γ_0

569 R: $\alpha(T_e - T_{s0})ac$

570 Λ: $p\kappa\gamma^*$

571

Appendix II: A nondimensional analysis of the dynamic system

With the nonlinear profile shown in Eq. (6) replaced by a linear profile shown in Eq. (9), the equations governing the behavior of the system are

$$\frac{dT_1}{dt} = c(T_e - T_1) + sq(T_2 - T_1) \quad \text{(A1)}$$

$$\frac{dT_2}{dt} = c(T_e - T_2) + q(T_{sub} - T_2) \quad \text{(A2)}$$

$$q = \frac{\alpha}{a}(T_1 - T_2) \quad \text{(A3)}$$

$$T_{sub} = T_{s0} + \gamma h_2^{'} \quad \text{(A4)}$$

$$T_{s0} = \lambda T_e + (1-\lambda)T_b \quad \text{(A5)}$$

$$\gamma = \gamma^* \frac{T_e - T_{s0}}{H_2} \quad \text{(A6)}$$

$$h_2^{'} - h_1^{'} = -\frac{H_1}{H_2} H \frac{\alpha}{b^2}(T_1 - T_2) \quad \text{(A7)}$$

$$\frac{1}{r}\frac{dh_1^{'}}{dt} = -h_1^{'} + \frac{H_1}{2H_2} H \frac{\alpha}{b^2}(T_1 - T_2) \quad \text{(A8)}$$

By introducing $\tau = ct$, $T_1^* = (T_1 - T_e)/T_e - T_{s0}$, $T_2^* = (T_2 - T_e)/T_e - T_{s0}$, $T_s^* = (T_{sub} - T_e)/T_e - T_{s0}$, $q^* = q/c$, $\gamma^* = \gamma H_2/(T_e - T_{s0})$, $h_1^{'*} = h_1^{'}/H_2$, and $h_2^{'*} = h_2^{'}/H_2$, we have the nondimensional form of (A1) - (A8) as,

$$\frac{dT_1^*}{d\tau} = -T_1^* + sq^*(T_2^* - T_1^*) \quad \text{(A9)}$$

$$\frac{dT_2^*}{d\tau} = -T_2^* + q^*(T_s^* - T_2^*) \quad \text{(A10)}$$

$$\frac{dh_1^{'*}}{d\tau} = -\sigma[h_1^{'*} - p\kappa R(T_1^* - T_2^*)] \quad \text{(A11)}$$

$$q^* = R(T_1^* - T_2^*) \quad \text{(A12)}$$

$$T_s^* = -1 + \gamma^* h_2^{'*} \quad \text{(A13)}$$

$$h_2^{'*} = h_1^{'*} - 2p\kappa R(T_1^* - T_2^*) \quad \text{(A14)}$$

where $R = \alpha(T_e - T_{s0})/ac$, $\kappa = ac/b^2$, $\sigma = r/c$, and $p = H_1/2H_2(1 + H_1/H_2)$. Plugging (A12) - (A14) into (A9) - (A11), and replacing $\gamma^* h_1^{'*}$ by η_1^* and $\gamma^* h_2^{'*}$ by η_2^*, we have

$$\frac{dT_1^*}{d\tau} = -T_1^* - sR(T_2^* - T_1^*)^2 \quad \text{(A15)}$$

$$\frac{dT_2^*}{d\tau} = -T_2^* + R(T_1^* - T_2^*)[-1 + \eta^* - 2\Lambda R(T_1^* - T_2^*) - T_2^*] \quad \text{(A16)}$$

$$\frac{1}{\sigma}\frac{d\eta_1^*}{d\tau} = -\eta_1^* + \Lambda R(T_1^* - T_2^*) \quad \text{(A17)}$$

$$T_s^* = -1 + \eta_2^* \quad \text{(A18)}$$

$$\eta_2^* = \eta_1^* - 2\Lambda R(T_1^* - T_2^*) \quad \text{(A19)}$$

where $\Lambda = p\kappa\gamma^*$. After such a manipulation to consolidate the parameters, we see that the dynamic behavior of the coupled system is determined by four non-dimensional parameters: R, Λ, σ and s.

Appendix III: An analysis of the relationship among the time-mean solution, the equilibrium solution, and the amplitude of the anomaly about the time-mean.

a. The equilibrium solutions

The equilibrium solutions can be obtained by setting the time derivatives on the left side of (A1), (A2), and (A8) to zero, and then reducing (A1) - (A8) to a single nonlinear algebraic equation. Here we only present the case for s=0. With s=0, (A1) - (A8) can be rewritten as

$$T_{1eq} = T_e \tag{A20}$$

$$c(T_e - T_{2eq}) + \frac{\alpha}{a}(T_{1eq} - T_{2eq})(T_{s0} + \gamma^* \frac{T_e - T_{s0}}{H_2} h'_{2eq} - T_{2eq}) = 0 \tag{A21}$$

$$q_{eq} = \frac{\alpha}{a}(T_{1eq} - T_{2eq}) \tag{A22}$$

$$h'_{2eq} = -\frac{H_1}{2H_2} H \frac{\alpha}{b^2}(T_{1eq} - T_{2eq}) \tag{A23}$$

$$h'_{1eq} = \frac{H_1}{2H_2} H \frac{\alpha}{b^2}(T_{1eq} - T_{2eq}) \tag{A24}$$

(The subscript 'eq' denotes the corresponding equilibrium solution of each variable.)

Plugging (A20), (A23) into equation (A21), we have

$$c(T_e - T_{2eq}) + \frac{\alpha}{a}(T_e - T_{2eq})(T_{s0} + \gamma^* \frac{T_e - T_{s0}}{H_2} \cdot \frac{-H_1}{2H_2} H \frac{\alpha}{b^2}(T_e - T_{2eq}) - T_{2eq}) = 0$$

$$\rightarrow \frac{ac}{\alpha} + T_{s0} + \gamma^* \frac{T_e - T_{s0}}{H_2} \cdot \frac{H_1}{2H_2} H \frac{\alpha}{b^2}(T_{2eq} - T_e) - T_{2eq} = 0 \tag{A25}$$

By introducing the nondimensional parameters R, Λ, p, κ, σ, (A25) can be rewritten as

$$\frac{ac}{\alpha} + T_{s0} + \Lambda R(T_{2eq} - T_e) - T_{2eq} = 0$$

$$\rightarrow T_{2eq} = \frac{\frac{ac}{\alpha} + T_{s0} - \Lambda R \cdot T_e}{1 - \Lambda R} \tag{A26}$$

626 Equations (A20) and (A26) are the equilibrium solutions of the linear system.

627

628 *b. Relationship among the time-mean solution, the equilibrium solution, and the*
629 *amplitude of the anomaly about the time-mean.*

630 As a variable (e.g. T) in its oscillatory state can be decomposed into its
631 climatological mean ($\overline{T}$) and corresponding fluctuating part (T'), the western and
632 eastern equatorial Pacific SST can be respectively written as: $T_1 = \overline{T_1} + T_1'$, $T_2 = \overline{T_2} + T_2'$,
633 also $h_2' = \overline{h_2'} + h_2''$. The difference between the two solutions can be expressed either in
634 the dimensional and nondimensional forms. Here we only present the derivation in
635 the dimensional form, and only refer the non-dimensional form of the equations when
636 asymptotic approximation is needed to obtain a clearer relation among the time-mean
637 value, the equilibrium value, and the amplitude of the anomalies about the time-mean.

638 We do time average to both the two sides of (A1), (A2), (A7), and (A8) in the
639 case $s = 0$, and also combine equations (A3) - (A6), then we have,

640 $$\overline{\frac{dT_1}{dt}} = \overline{c(T_e - T_1)} \tag{A27}$$

641 $$\overline{\frac{dT_2}{dt}} = \overline{c(T_e - T_2)} + \overline{\frac{\alpha}{a}(T_1 - T_2)(T_{s0} + \gamma h_2' - T_2)} \tag{A28}$$

642 $$\overline{h_2'} - \overline{h_1'} = -\frac{H_1}{H_2} H \frac{\alpha}{b^2}(\overline{T_1} - \overline{T_2}) \tag{A29}$$

643 $$\overline{\frac{1}{r}\frac{dh_1'}{dt}} = -\overline{h_1'} + \frac{H_1}{2H_2} H \frac{\alpha}{b^2}(\overline{T_1} - \overline{T_2}) \tag{A30}$$

644 Simplify (A27) - (A30), we can get

645 $$\overline{T_1} = T_e \tag{A31}$$

646 $$\overline{c(T_e - T_2)} + \overline{\frac{\alpha}{a}(T_1 - T_2)(T_{s0} + \gamma h_2' - T_2)} = 0 \tag{A32}$$

647 $$\overline{h_2'} = -\frac{H_1}{2H_2} H \frac{\alpha}{b^2}(\overline{T_1} - \overline{T_2}) \tag{A33}$$

$$\overline{h_1^{'}} = \frac{H_1}{2H_2} H \frac{\alpha}{b^2} (\overline{T_1} - \overline{T_2}) \tag{A34}$$

Simplify (A32), we have

$$cT_e - c\overline{T_2} + \overline{\frac{\alpha}{a}(\overline{T_1} - \overline{T_2} + T_1^{'} - T_2^{'})(T_{s0} + \gamma \overline{h_2^{'}} - \overline{T_2} + \gamma h_2^{''} - T_2^{'}) = 0}$$

$$\rightarrow \frac{ac}{\alpha}(T_e - \overline{T_2}) + \left(\overline{(\overline{T_1} - \overline{T_2}) \cdot (T_{s0} + \gamma \overline{h_2^{'}} - \overline{T_2})} + \overline{(T_1^{'} - T_2^{'})(\gamma h_2^{''} - T_2^{'})} \right) = 0 \tag{A35}$$

As we can easily get $\overline{T_1} = T_{eq} = T_e$ due to a combination of (A20) and (A31), and there is no oscillation for T_1 at this time, $T_1^{'} = 0$. Also by combining (A33), equation (A35) can be further simplified as,

$$\frac{ac}{\alpha}(T_e - \overline{T_2}) + (T_e - \overline{T_2}) \cdot (T_{s0} + \gamma^* \frac{T_e - T_{s0}}{H_2} \cdot \frac{-H_1}{2H_2} H \frac{\alpha}{b^2} (\overline{T_1} - \overline{T_2}) - \overline{T_2}) + \overline{(-T_2^{'})(\gamma h_2^{''} - T_2^{'})} = 0$$

$$\rightarrow \frac{ac}{\alpha}(T_e - \overline{T_2}) + (T_e - \overline{T_2}) \cdot (T_{s0} + \Lambda R(\overline{T_2} - T_e)^2 - \overline{T_2}) + \overline{(-T_2^{'})(\gamma h_2^{''} - T_2^{'})} = 0$$

$$\rightarrow \frac{ac}{\alpha} + T_{s0} + (\Lambda R - 1)\overline{T_2} - \Lambda R \cdot T_e + \frac{\overline{(-T_2^{'})(\gamma h_2^{''} - T_2^{'})}}{T_e - \overline{T_2}} = 0$$

$$\rightarrow \overline{T_2} = \frac{\frac{ac}{\alpha} + T_{s0} - \Lambda R \cdot T_e}{1 - \Lambda R} + \frac{\overline{\gamma h_2^{''} T_2^{'} - T_2^{'2}}}{(\Lambda R - 1) \cdot (T_e - \overline{T_2})} \tag{A36}$$

As shown by (A26), $T_{2eq} = \frac{\frac{ac}{\alpha} + T_{s0} - \Lambda R \cdot T_e}{1 - \Lambda R}$, the relationship between $\overline{T_2}$ and T_{2eq} is

$$\overline{T_2} = T_{2eq} + \frac{\overline{\gamma h_2^{''} T_2^{'} - T_2^{'2}}}{(\Lambda R - 1) \cdot (T_e - \overline{T_2})} \tag{A37}$$

As we get easily get $T_{sub}^{'} = \gamma h_2^{"}$, (recall $T_{sub} = T_{s0} + \gamma h_2^{'}$ (A4)), (A37) can be rewritten as

$$\overline{T_2} = T_{2eq} + \frac{\overline{T_{sub}^{'} T_2^{'}} - \overline{T_2^{'2}}}{(\Lambda R - 1)(T_e - \overline{T_2})} \tag{A38}$$

When $\sigma = \frac{r}{c} >> 1$, equation (A17) becomes $\eta_1^* = \Lambda R(T_1^* - T_2^*)$. As $T_1^* = 0\,(s = 0)$ at this time, combining equations (A18) and (A19), we can get $T_s^* + 1 = \Lambda R T_2^*$. We

667 can further get $T_{sub}{}' = \Lambda R T_2{}'$ easily as we return it to its dimensional form. (A38) can
668 thereby be derived as

669 $$\overline{T_2} = T_{2eq} + \frac{\overline{T_2{}'^2}}{T_e - \overline{T_2}} \tag{A39}$$

670 Recall in this particular case $\overline{T_1} = T_e$, we have

671 $$\overline{T_2} = T_{2eq} + \frac{\overline{T_2{}'^2}}{\overline{T_1} - \overline{T_2}} \tag{A40}$$

672 The simple advective case (that the eastern Pacific is periodically invaded or flooded
673 by an expanding warmpool (Fig. 9) appears to satisfy this equation,
674 with $\tilde{T}'_2 \sim \overline{T_1} - \overline{T_2} = \frac{1}{2}(T_{1eq} - T_{2eq})$, $\overline{T_1} \sim T_{1eq}$, $\overline{T_2} \sim \frac{1}{2}(T_{1eq} + T_{2eq})$, $\tilde{T}'_2$ is the magnitude of
675 the anomaly above the time-mean ($\sqrt{\tilde{T}'^2_2}$)

676 For a more general case, we take $T_2{}' = A\cos\omega t$, $T_{sub}{}' = \Lambda R A\cos(\omega t - \beta)$ ($\beta > 0$),

$$\begin{aligned} T_{sub}{}' T_2{}' &= \Lambda R\left[A^2\cos\omega t\cdot\cos(\omega t-\beta)\right] \\ &= \Lambda R\left[A^2\cos\omega t(\cos\omega t\cos\beta+\sin\omega t\sin\beta)\right] \\ &= \Lambda R\left[A^2\cos^2\omega t\cos\beta + A^2\cos\omega t\sin\omega t\sin\beta\right] \end{aligned}$$

677

678 $$\overline{T_{sub}{}' T_2{}'} = \Lambda R\overline{A^2\cos^2\omega t\cos\beta} = \Lambda R\cos\beta\,\overline{T_2{}'^2}$$

679 Equation (A38) becomes $\overline{T_2} = T_{2eq} + \frac{\Lambda R\cos\beta - 1}{\Lambda R - 1}\frac{\overline{T_2{}'^2}}{\overline{T_1} - \overline{T_2}}$ (A41)

680 When $\Lambda R >> 1$, equation (A41) becomes

681 $$\overline{T_2} = T_{2eq} + \cos\beta\frac{\overline{T_2{}'^2}}{\overline{T_1} - \overline{T_2}} \tag{A42}$$

682 Note,

683 $$\Lambda R = p\kappa\gamma^* R = {}^{H_1}\!/_{2H_2}\,(1 + {}^{H_1}\!/_{H_2})\cdot\frac{ac}{b^2}\cdot\frac{\gamma H_2}{T_e - T_{s0}}\cdot\alpha\frac{T_e - T_{s0}}{ac} = \frac{H_1 H}{2H_2}\frac{\alpha\gamma}{b^2} \tag{A43}$$

684 Therefore (A42) corresponds to the case with a very strong Bjerknes feedback. Recall
685 that α and γ in (A43) are respectively the coupling strength and the lapse rate of
686 the thermocline (Appendix I).

687
688

689 **ACKNOWLEDGEMENTS**

690

691 The authors would like to thank University of Colorado at Boulder for hosting Jin
692 Liang for his visit. The research was supported by the National Natural Science
693 Foundation of China (NSFC) under grants No. 40730953 and 40805025, and by
694 US NSF grant AGS 0852329 and by grants from NOAA office of global programs.

695

696

697 **REFERENCE**

698

699 An, S.-I., and F.-F. Jin, 2001: Collective role of thermocline and zonal advective
700 feedbacks in the ENSO mode. *J. Climate*, **14,** 3421-3432.

701 ——, and ——, 2004: Nonlinearity and asymmetry of ENSO. *J. Climate*, **17,**
702 2399-2412.

703 ——, Y.-G. Ham, J.-S.Kug, F.-F. Jin, and I.-S. Kang, 2005: El Niño - La Niña
704 asymmetry in the coupled model intercomparison project simulations. *J. Climate*,
705 **18,** 2617-2627.

706 Burgers, G., and D. B. Stephenson, 1999: The "normality" of El Niño. *Geophys. Res.*
707 *Lett.*, **26,** 1027-1030, doi:10.1029/1999GL900161.

708 Cane, M. A., A. C. Clement, A. Kaplan, Y. Kushnir, D. Pozdnyakov, R. Seager, S. E.
709 Zebiak, and R. Murtugudde, 1997: Twentieth-century sea surface temperature
710 trends. *Science*, **275,** 957-960.

711 Clement, A. C., R. Seager, M. A. Cane, and S. E. Zebiak, 1996: An ocean dynamical
712 thermostat. *J. Climate*, **9,** 2190-2196.

713 Collins, M., and Coauthors, 2010: The impact of global warming on the tropical
714 Pacific ocean and El Niño. *Nat. Geosci.*, **3,** 391-397.

715 Fedorov, A. V., and S. G. Philander, 2000: Is El Niño changing? *Science*, **288,**
716 1997-2002.

717 ——, and ——, 2001: A stability analysis of tropical ocean-atmosphere interactions:
718 Bridging measurements and theory for El Niño. *J. Climate*, **14**, 3086-3101.

719 Flugel, M., Chang, P. & Penland, C. 2004 Identification of dynamical regimes in an
720 intermediate coupled ocean–atmosphere model. J. Climate, 13, 2105–2115.

721 Guilyardi, E., A. Wittenberg, A. Fedorov, M. Collins, C. Wang, A. Capotondi, G. J.
722 van Oldenborgh, and T. Stockdale, 2009: Understanding El Niño in
723 ocean-atmosphere general circulation models. *Bull. Amer. Meteor. Soc.*, **90,**
724 325-340, doi:10.1175/2008BAMS2387.1.

725 ——, W. J. Cai, M. Collins, A. Fedorov, F.-F. Jin, A. Kumar, D.-Z. Sun, A.
726 Wittenberg, 2011: New strategies for evaluating ENSO processes in climate
727 models. *BAMS*, Submitted.

728 Gent, P. R., and M. A. Cane, 1989: A reduced gravity, primitive equation model of
729 the upper equatorial ocean. *Comp. Phys.*, **81**, 444-480.

730 Jin, F.-F., 1996: Tropical ocean interaction, Pacific cold tongue, and El Niño Southern
731 Oscillation. *Science*, **274,** 76–78.

732 ——, 1997: An equatorial ocean recharge paradigm for ENSO. Part I: conceptual
733 model. *J. Atmos. Sci.*, **54,** 811-829.

734 ——, S.-I. An, A. Timmermann, and J. X. Zhao, 2003: Strong El Niño events and
735 nonlinear dynamical heating. *Geophys. Res. Lett.*, **30,** 1120,
736 doi:10.1029/2002GL016356.

737 Kleeman, R. 2008: Stochastic theories for the irregularity of ENSO. *Phil. Trans. Roy.*
738 *Soc. A.*, 366:2509-2524.

739 Manabe, S., and R. F., Moller, 1961: On the radiative equilibrium and the heat
740 balance of the atmosphere. *Mon. Wea. Rev.*, **89,** 503-532.

741 ——, and ——, 1964: Thermal equilibrium of the atmosphere with convective

742 adjustment. *J. Atmos. Sci.*, **21,** 361-385.

743 ——, and R. T. Wetherald, 1967: Thermal equilibrium of the atmosphere with a given
744 distribution of relative humidity. *J. Atmos. Sci.*, **24,** 241-259.

745 Meehl, G. A., A. Hu, C. Tebaldi, 2010: Decadal prediction in the Pacific region. *J.*
746 *Climate*, **23**, 2959-2973.

747 Moor, A., and R. Kleeman, 1999: Stochastic Forcing of ENSO by the Intraseasonal
748 Oscillation. *J. Climate*, **23**, 2959-2973.

749 Penland, C., 1996: A stochastic model of IndoPacific sea surface temperature
750 anomalies. *Physica D*, 98, 534–558.

751 ——, and P. D. Sardeshmukh, 1995: The optimal growth of tropicalsea surface
752 temperature anomalies. *J. Climate*, **8**, 1999–2024.

753 Philander, S. G., 1990: *El Niño, La Niña, and the Southern Oscillation.* Academic
754 Press, 293 pp.

755 Picaut, J., F. Masia and Y. du Penhoat, 1997: An advective-reflective conceptual
756 model for the oscillatory nature of the ENSO. *Science*, **277,** 663-666.

757 Rayner, N. A., E. B. Horton, D. E. Parker, C. K. Folland, and R. B. Hackett, 1996:
758 Version 2.2 of the Global sea-ice and Sea Surface Temperature data set,
759 1903-1994. September 1996, Climate Research, Technical Note 74 (CRTN74),
760 Hadley Centre for Climate Prediction and Research, Meteorological Office,
761 London Road, Bracknell, Berkshire RG12 2SY.

762 Rodgers, K. B., P. Friederichs, and M. Latif, 2004: Tropical Pacific decadal
763 variability and its relation to decadal modulations of ENSO. *J. Climate*, **17,**
764 3761-3774.

765 Schopf, P. S., and R. J. Burgman, 2006: A simple mechanism for ENSO residuals and
766 asymmetry. *J. Climate*, **19,** 3167-3179.

767 Strogatz, S., 2001: *Non-linear Dynamics and Chaos: With applications to Physics,*
768 *Biology, Chemistry and Engineering*, Westview Press, 528 pp.

769 Sun, D.-Z., 1997: El Niño: A coupled response to radiative heating? *Geophys. Res.*
770 *Lett*, **24,** 2031-2034, doi:10.1029/97GL01960.

771 ——, 2000: Global climate change and ENSO: A theoretical framework. *El Niño:*
772 *Historical and Paleoclimatic Aspects of the Southern Oscillation, Multiscale*
773 *variability and Global and Regional Impacts*, H. F. Diaz and V. Markgraf, Eds.,
774 Cambridge University Press, 443-463.

775 ——, 2003: A possible effect of an increase in the warm - pool SST on the magnitude
776 of El Niño warming. *J. Climate*, **16,** 185-205.

777 ——, 2010: The diabatic and nonlinear aspects of El Niño - Southern Oscillation:
778 Implications for its past and future behavior, in *AGU Geophysical Monograph*
779 *"Climate Dynamics: Why Does Climate Vary?"*, edited by D.-Z. Sun. and F.
780 Bryan, pp.79-104, AGU, Washington, D. C.

781 ——, and T. Zhang, 2006: A regulatory effect of ENSO on the time - mean thermal
782 stratification of the equatorial upper ocean. *Geophys. Res. Lett.*, **33,** L07710,
783 doi:10.1029/2005GL025296.

784 ——, ——, C. Covey, S. A. Klein, W. D. Collins, J. J. Hack, J. T. Kiehl, G.A. Meehl,
785 I. M. Held, and M. Suarez, 2006: Radiative and dynamical feedbacks over the
786 equatorial cold-tongue: results from nine atmospheric GCMs. *J. Climate*, **19,**
787 4059-4074.

788 ——, and Z. Liu, 1996: Dynamic ocean-atmosphere coupling: a thermostat for the

789 tropics. *Science*, **272,** 1148-1150.

790 Sun, F. P., J.-Y. Yu, 2009: A 10-15-yr modulation cycle of ENSO intensity. *J.*
791 *Climate*, **22,** 1718-1735.

792 Sun, Y., L. Wu, and D.-Z. Sun, 2011: Evidence from climate models for ENSO events
793 in shaping the tropical mean climate. *J. Climate,* Submitted.

794 Timmermann, A., and F.-F. Jin, 2002: A nonlinear mechanism for decadal El Niño
795 amplitude changes. *Geophys. Res. Lett.*, **29,** 1003, doi:10.1029/2001GL013369.

796 Vecchi, G. A., A. Clement, and B. J. Soden, 2008: Examining the tropical Pacific's
797 response to global warming. *Eos, Trans. Amer. Geophys. Union,* **89** (9), 81-83.

798 Wang, B., and S.-I. An, 2001: Why the properties of El Niño changed during the late
799 1970s. *Geophys. Res. Lett.*, **28,** 3709-3712.

800 Wang, X. L., and C.-F. Ropelewski, 1995: An assessment of ENSO-scale secular
801 variability. *J. Climate*, **8,** 1584-1589.

802 Wittenberg, A. T., 2009: Are historical records sufficient to constrain ENSO
803 simulations? *Geophys. Res. Lett.*, **36,** L12702, doi:10.1029/2009GL038710.

804 Xu, K.-M., and K. A. Emanuel, 1989: Is the tropical atmosphere conditionally
805 unstable? *Mon. Wea. Rev.*, **117,** 1471-1479.

806 Zebiak, S. E., and M. A. Cane, 1987: A model El Niño - Southern Oscillation. *Mon*
807 *Weather Rev*, **115,** 2262-2278.

808 Zhang, T., D.-Z. Sun, R. Neale, and P. J. Rasch, 2009: An evaluation of ENSO
809 asymmetry in the Community Climate System Models: A view from the
810 subsurface. *J. Climate*, **22**, 5933–5961.

811

812 Zhang, Y., J. M. Wallace, and D. S. Battisti, 1997: ENSO-like interdecadal
813 variability: 1900-93. *J. Climate*, **10,** 1004-1020.

814

815

816 **Figure Captions:**

817

818 **FIG. 1.** (a) Sea Surface Temperature (SST) differences between two epochs:
819 1977–2003 and 1950–1976. (b) Niño3 SST time series. Niño3 SST (anomalies) (in
820 color). The black solid line is the variance of Niño3 SST anomalies obtained by
821 sliding a moving window of a width of 16 years. Note the epoch 1977–2003 has
822 higher level of ENSO activity than the previous period 1950–1976. (SST data used
823 are from the Hadley Center for Climate Prediction and Research) (Rayner et al. 1996).

824

825 **FIG. 2.** (a) Equatorial Pacific SST as a function of T_e. T_1 and T_2 are respectively for
826 the western and eastern Pacific SST. Solid lines are for the time-mean state, and the
827 dashed lines are for the equilibrium state. (b) Amplitude of oscillation for T_2 as a
828 function of T_e. The amplitude is defined here as the half value of the difference
829 between the maximum and minimum value of T_2. Also shown are the zonal SST
830 contrast as measured by the difference between T_1 and T_2 for the equilibrium state
831 (red) and the time-mean state (blue). Note that the rate of increase in the zonal
832 contrast in the time-mean state with T_e is less than half of the corresponding rate of
833 increase in the equilibrium state (0.25 versus 0.56). The parameter values used in this
834 figure are the same as in Sun (1997, 2000) (s=1/3, T_b=17.3°C, $\frac{1}{c}=150day$,
835 $\frac{1}{r}=300day$, $H^*=65m$, $H_1=50m$, $H_2=150m$, $z_0=75m$, $\frac{\alpha}{a}=3.0\times10^{-8}K^{-1}s^{-1}$,
836 $\frac{H_1(H_1+H_2)}{2H_2}\cdot\frac{\alpha}{b^2}=11.5mK^{-1}$)

837

838 **FIG. 3**. Same as in Fig. 2a except for the subsurface temperature (a), the upwelling

(b), the thermocline depth of the eastern equatorial Pacific (anomaly) (c), and the depth of the thermocline in the western equatorial Pacific (anomaly) (d). Note that a negative anomaly in h_2' means a reduction in the thermocline depth. The positive difference between the time-mean solution of h_2' and the equilibrium h_2' in the presence of ENSO implies a deepening of h_2' in the eastern Pacific due to the presence of ENSO.

FIG. 4. Same as in Fig. 2, except for s=0 (a, b) and s=0.096 (c, d).

FIG. 5. Time series of T_2 when T_e=28.5°C and T_e=31°C. The time series are taken from the case with s=0.096 (Fig. 4cd). The two horizontal lines in the figure indicate respectively the time-mean value of T_2 *(solid line) and its equilibrium value (dashed line).*

FIG. 6. (a) The time series of h_1', corresponding to the time series of T_2 shown in Fig.5b. The time mean value and the equilibrium value of h_1' are also plotted in the figure—the solid and dashed horizontal lines. (b) The corresponding trajectory of the system, projected onto the plan of T_2 and h_1'. The small red circle and square in the figure mark the positions of the equilibrium and time-mean state respectively.

FIG. 7. Same as in Fig. 2a and 2b, but with the reference profile used to parameterize the subsurface temperature T_{sub} (Eq. (6)) replaced by $\Phi(z) = T_{s0} + \gamma(z + H_1)$, where $T_{s0} = \lambda T_e + (1-\lambda)T_b$ and $\gamma = (T_e - T_b)/2H_{ref}$. Parameter values used for this the linear profile are λ=17/24, H_{ref}=64m. Other parameters are the same as in Fig. 2.

FIG. 8. The profile for the reference subsurface temperature used to link the subsurface temperature to the depth of the thermocline for the linear case (Fig. 7) and the nonlinear case (Fig.2). Solid line is for the linear case, while dashed line is for the nonlinear case. Only the profile corresponding to T_e =29.5°C is plotted here.

FIG. 9. A schematic illustration of the simple advective model (a and b), in which El Nino event is viewed as a periodical (or episodical) "flooding" event of the eastern Pacific region – a region that is otherwise cold (when instability does not take place) --by warm water in the western Pacific. Fig. 7c shows the resulting time-mean state. In the situation of a sinusoidal expansion of the warm-pool, $\overline{T_1} \sim T_{1eq}$, $\overline{T_2} \sim \frac{1}{2}(T_{1eq} + T_{2eq})$, $\tilde{T}'_2 \sim \overline{T}_1 - \overline{T}_2 = \frac{1}{2}(T_{1eq} - T_{2eq})$ with $\tilde{T}'_2$ being the magnitude of T_2' or ENSO anomaly.

878

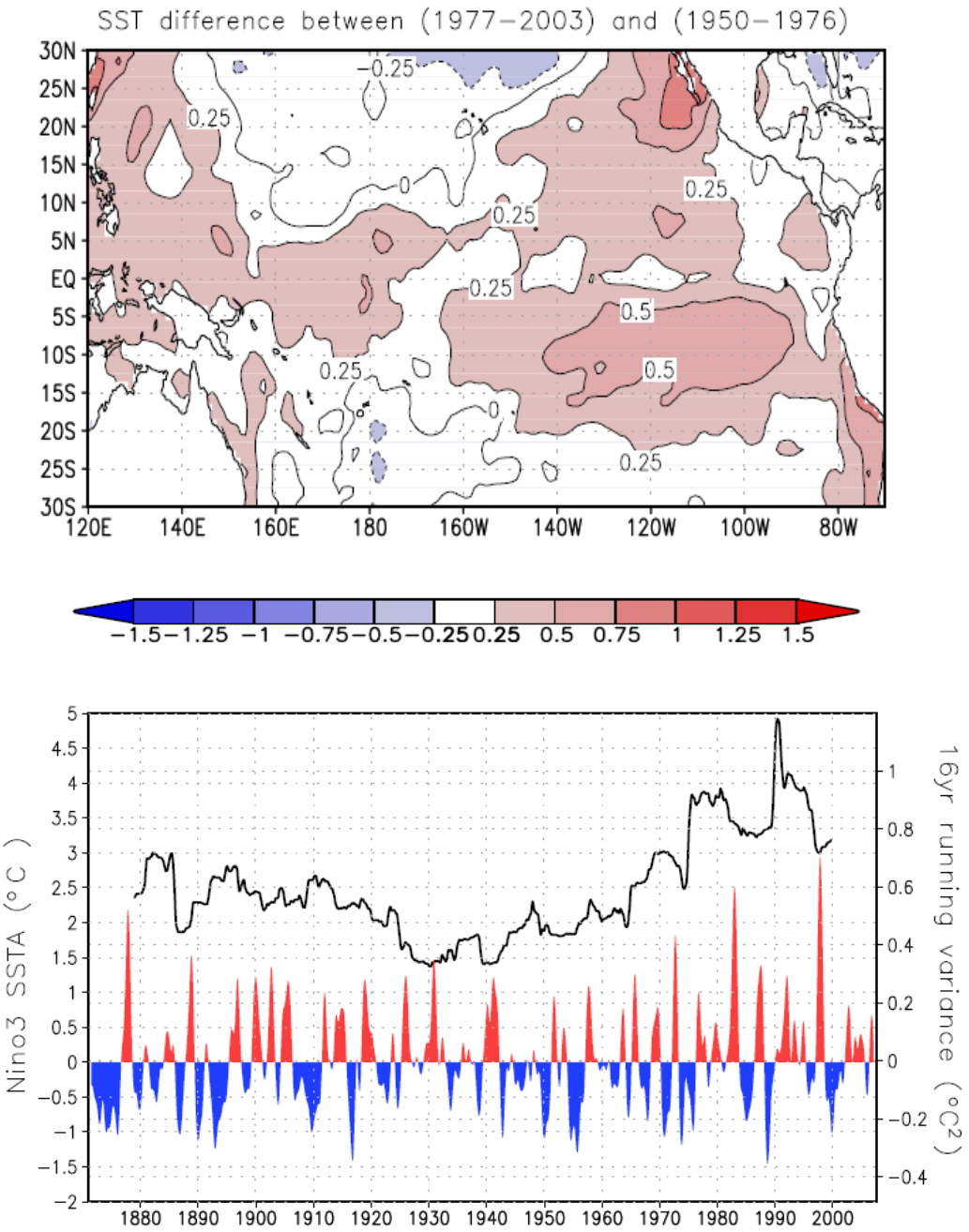

879

880

881 **FIG. 1.** (a) Sea Surface Temperature (SST) differences between two epochs:
882 1977–2003 and 1950–1976. (b) Niño3 SST time series. Niño3 SST (anomalies) (in
883 color). The black solid line is the variance of Niño3 SST anomalies obtained by
884 sliding a moving window of a width of 16 years. Note the epoch 1977–2003 has
885 higher level of ENSO activity than the previous period 1950–1976. (SST data used
886 are from the Hadley Center for Climate Prediction and Research) (Rayner et al. 1996).
887

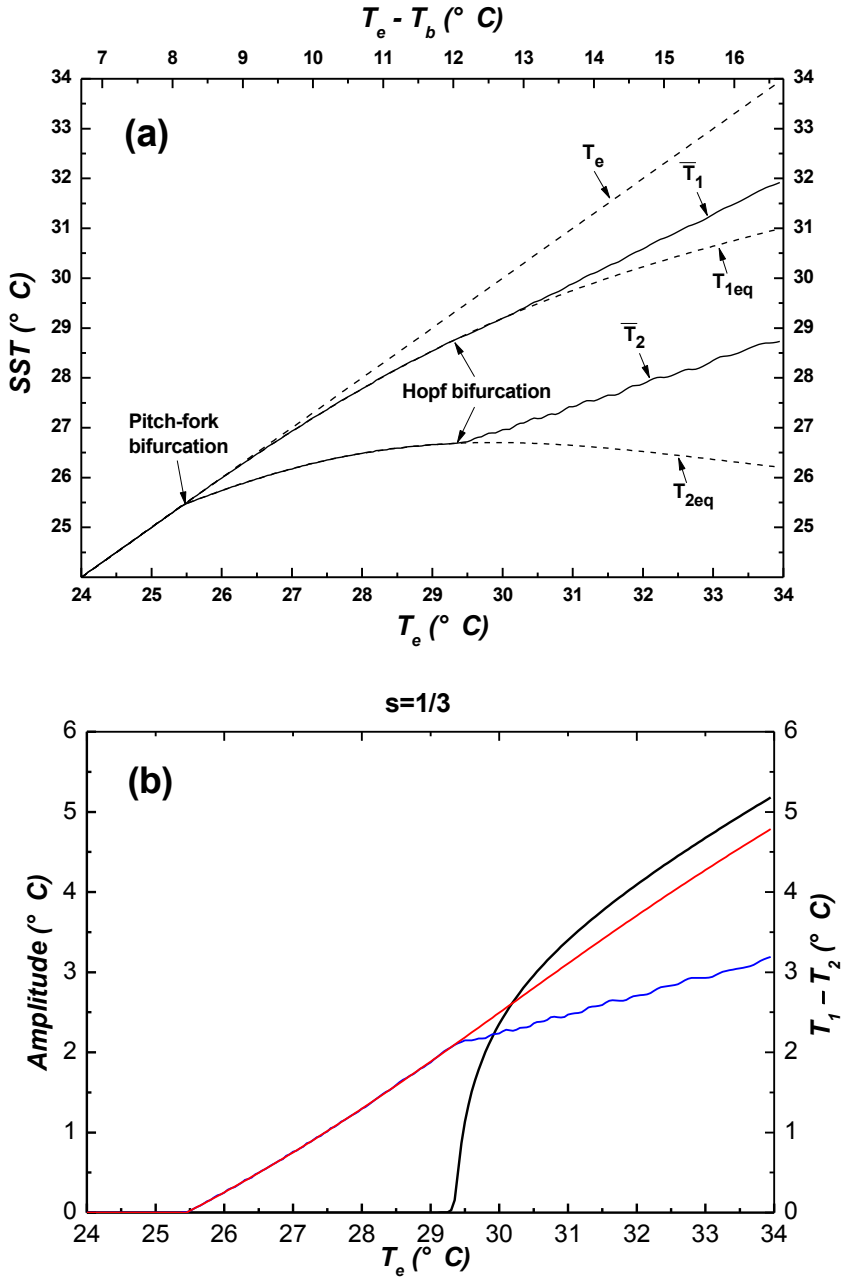

888

889

890 **FIG. 2.** (a) Equatorial Pacific SST as a function of T_e. T_1 and T_2 are respectively for
891 the western and eastern Pacific SST. Solid lines are for the time-mean state, and the
892 dashed lines are for the equilibrium state. (b) Amplitude of oscillation for T_2 as a
893 function of T_e. The amplitude is defined here as the half value of the difference
894 between the maximum and minimum value of T_2. Also shown are the zonal SST
895 contrast as measured by the difference between T_1 and T_2 for the equilibrium state
896 (red) and the time-mean state (blue). Note that the rate of increase in the zonal
897 contrast in the time-mean state with T_e is less than half of the corresponding rate of
898 increase in the equilibrium state (0.25 versus 0.56). The parameter values used in this
899 figure are the same as in Sun (1997, 2000) ($(s=1/3,\ T_b=17.3°C,\ \frac{1}{c}=150day,$
900 $\frac{1}{r}=300day,\ H^*=65m,\ H_1=50m,\ H_2=150m,\ z_0=75m,\ \frac{\alpha}{a}=3.0\times10^{-8}K^{-1}s^{-1},$

901 $$\frac{H_1(H_1+H_2)}{2H_2}\cdot\frac{\alpha}{b^2}=11.5mK^{-1})$$

902

903

904

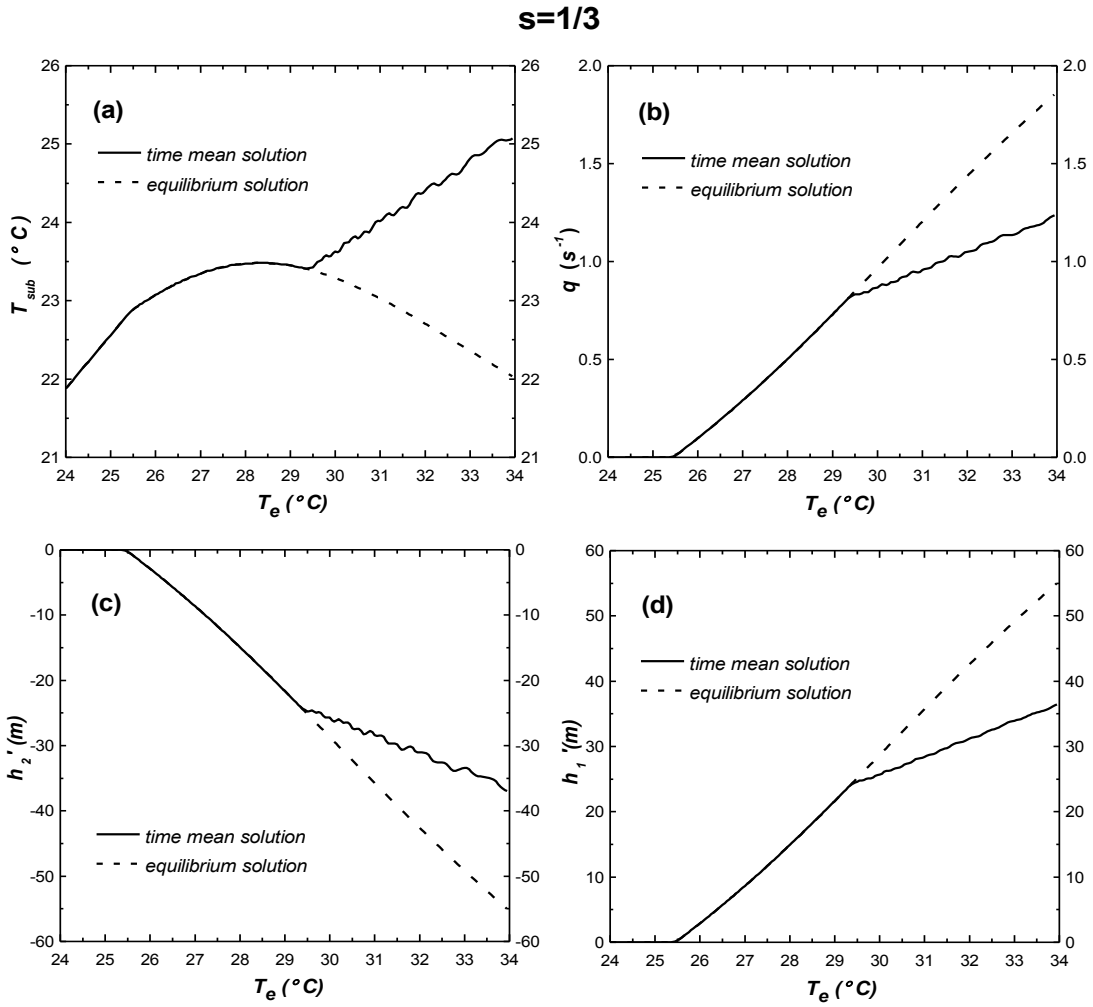

FIG. 3. Same as in Fig. 2a except for the subsurface temperature (a), the upwelling (b), the thermocline depth of the eastern equatorial Pacific (anomaly) (c), and the depth of the thermocline in the western equatorial Pacific (anomaly) (d). Note that a negative anomaly in h_2' means a reduction in the thermocline depth. The positive difference between the time-mean solution of h_2' and the equilibrium h_2' in the presence of ENSO implies a deepening of h_2' in the eastern Pacific due to the presence of ENSO.

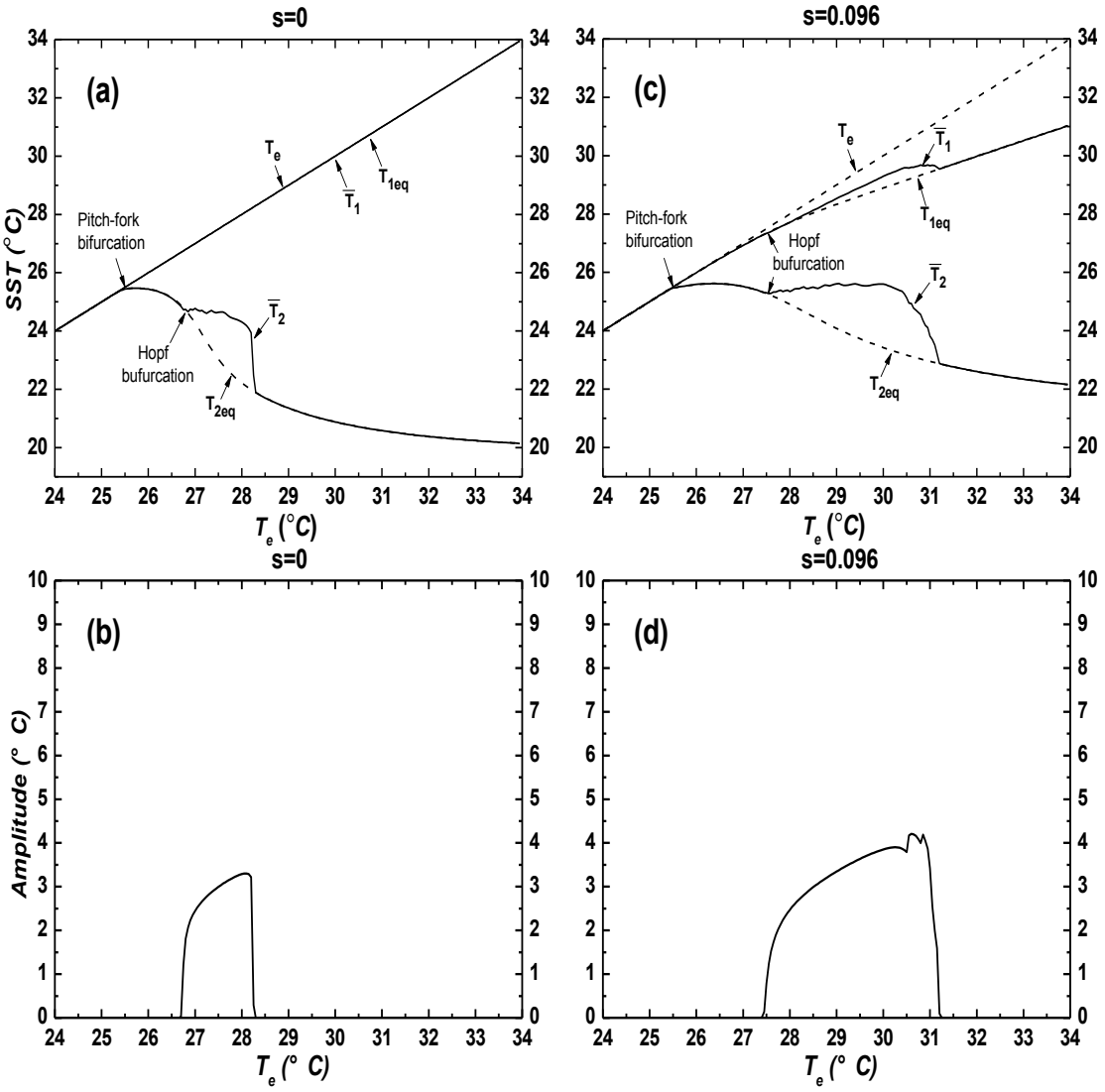

915

916

917 **FIG. 4.** Same as in Fig. 2, except for *s*=0 (a, b) and *s*=0.096 (c, d).

918

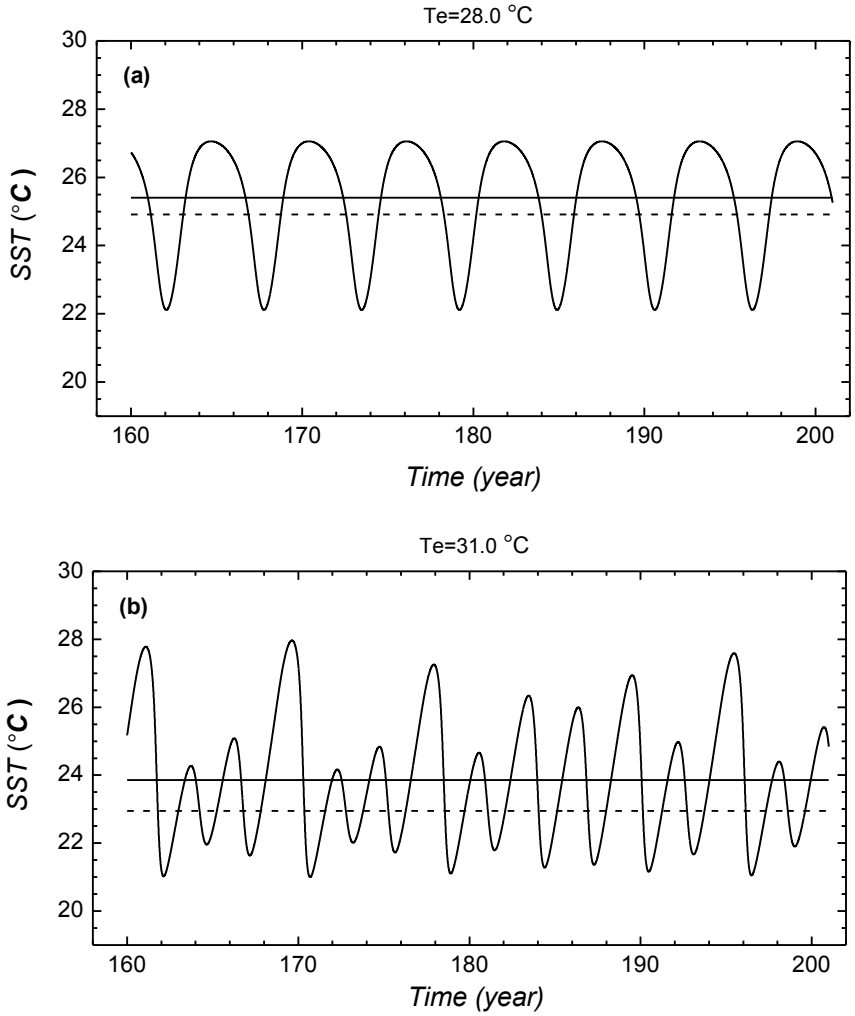

FIG. 5. Time series of T_2 when T_e=28.5°C and T_e=31°C. The time series are taken from the case with s=0.096 (Fig. 4cd). The two horizontal lines in the figure indicate respectively the time-mean value of T_2 *(solid line)* and its equilibrium value *(dashed line)*.

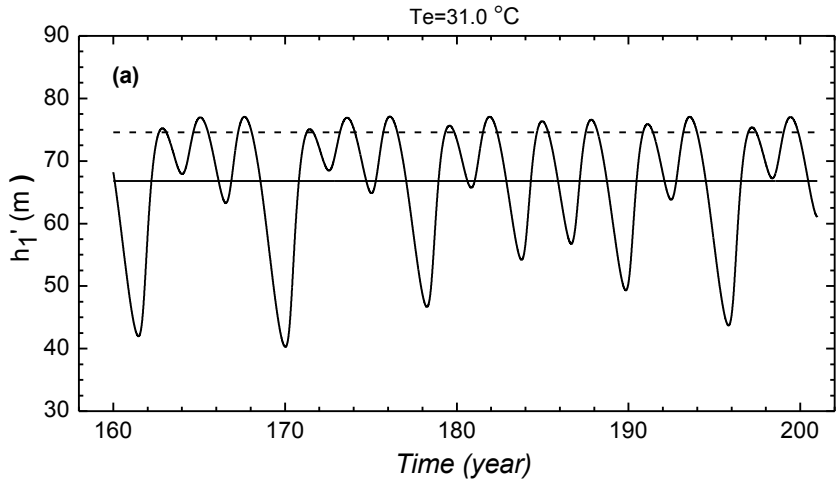

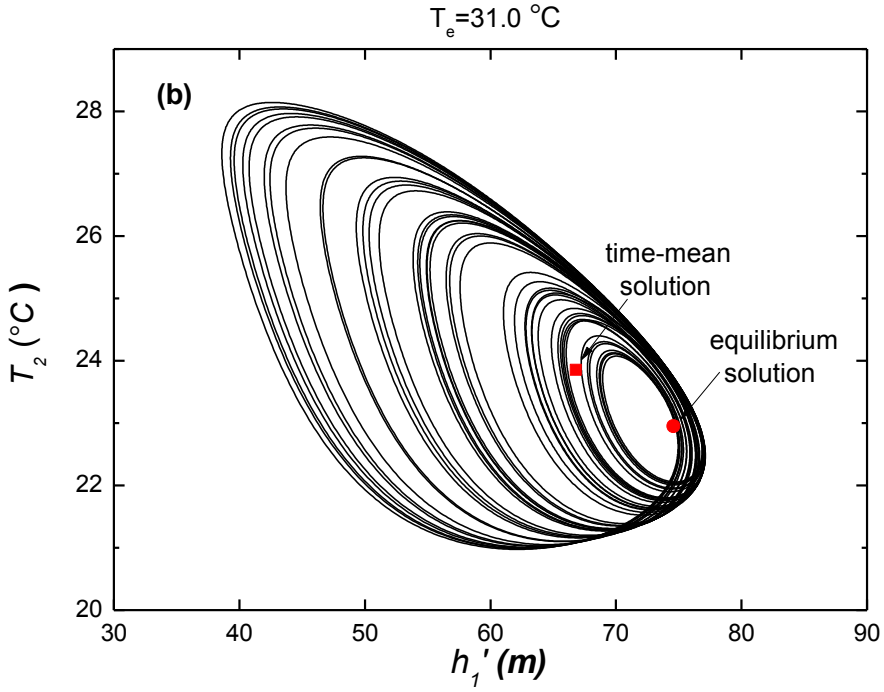

FIG. 6. (a) The time series of h_1', corresponding to the time series of T_2 shown in Fig.5b. The time mean value and the equilibrium value of h_1' are also plotted in the figure—the solid and dashed horizontal lines. (b) The corresponding trajectory of the system, projected onto the plan of T_2 and h_1'. The small red circle and square in the figure mark the positions of the equilibrium and time-mean state respectively

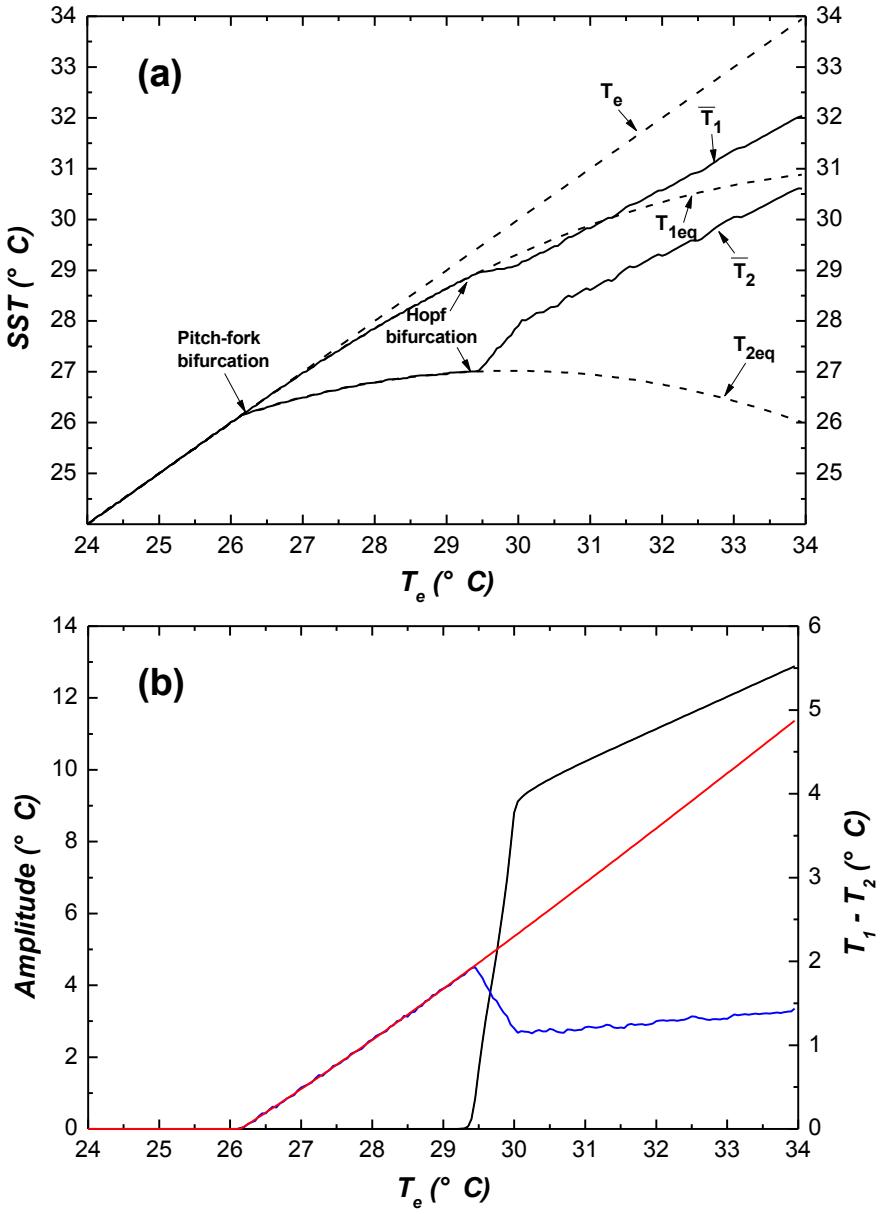

FIG. 7. Same as in Fig. 2a and 2b, but with the reference profile used to parameterize the subsurface temperature T_{sub} (Eq. (6)) replaced by $\Phi(z) = T_{s0} + \gamma(z + H_1)$, where $T_{s0} = \lambda T_e + (1-\lambda)T_b$ and $\gamma = (T_e - T_b)/2H_{ref}$. Parameter values used for this the linear profile are $\lambda = 17/24$, $H_{ref} = 64m$. Other parameters are the same as in Fig. 2.

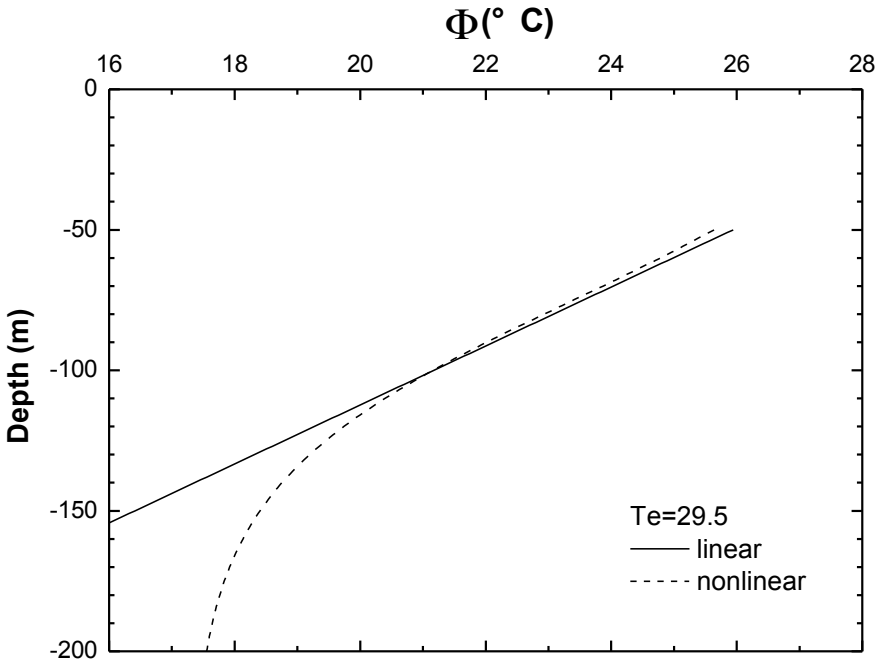

953
954
955 **FIG. 8.** The profile for the reference subsurface temperature used to link the
956 subsurface temperature to the depth of the thermocline for the linear case (Fig. 7) and
957 the nonlinear case (Fig.2). Solid line is for the linear case, while dashed line is for the
958 nonlinear case. Only the profile corresponding to T_e =29.5°C is plotted here.
959

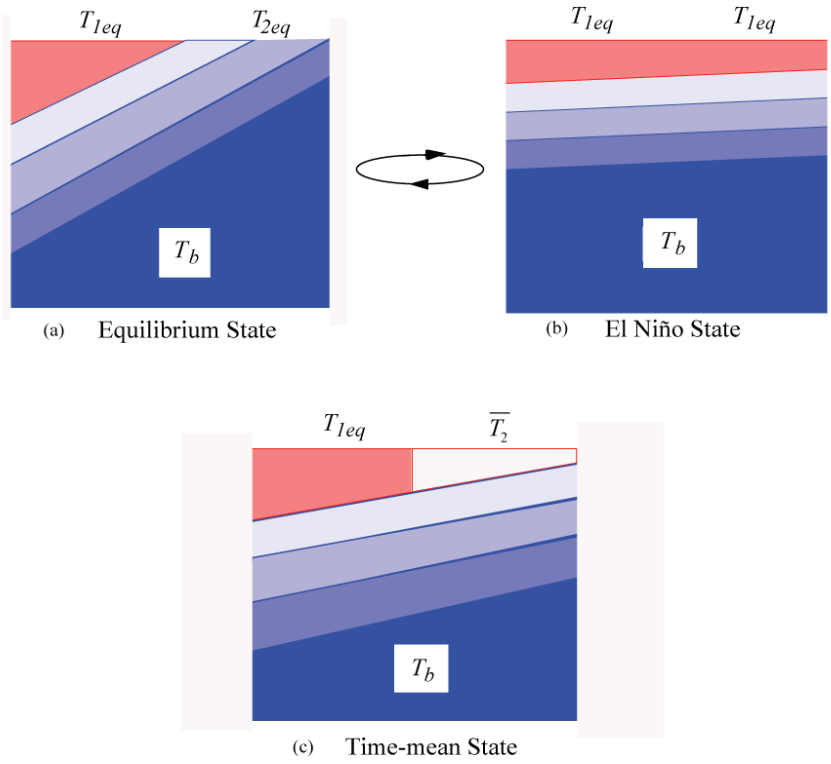

960
961
962

963 **FIG. 9.** A schematic illustration of the simple advective model (a and b), in which El
964 Nino event is viewed as a periodical (or episodical) "flooding" event of the eastern
965 Pacific region – a region that is otherwise cold (when instability does not take place) –
966 by warm water in the western Pacific. Fig.9c shows the resulting time-mean state. In
967 the situation of a sinusoidal expansion of the warm-pool, $\overline{T_1} \sim T_{1eq}$, $\overline{T_2} \sim \frac{1}{2}(T_{1eq} + T_{2eq})$,
968 $\tilde{T}'_2 \sim \overline{T}_1 - \overline{T}_2 = \frac{1}{2}(T_{1eq} - T_{2eq})$ with $\tilde{T}'_2$ being the magnitude of T_2' or ENSO anomaly.

969